Energy Conversion and Management 134 (2017) 188–196

Contents lists available at ScienceDirect

Energy Conversion and Management

journal homepage: www.elsevier.com/locate/enconman

Deoxygenation of palm kernel oil to jet fuel-like hydrocarbons using Ni-MoS_2/γ-Al_2O_3 catalysts

Vorranutch Itthibenchapong [a], Atthapon Srifa [a], Rungnapa Kaewmeesri [a], Pinit Kidkhunthod [b], Kajornsak Faungnawakij [a,*]

[a] Nanomaterials for Energy and Catalysis Laboratory, National Nanotechnology Center (NANOTEC), National Science and Technology Development Agency (NSTDA), 111 Thailand Science Park, Pathum Thani 12120, Thailand
[b] Synchrotron Light Research Institute (Public Organization), 111 University Avenue, Muang District, Nakhon Ratchasima 30000, Thailand

ARTICLE INFO

Article history:
Received 4 November 2016
Received in revised form 13 December 2016
Accepted 14 December 2016

Keywords:
Hydrodeoxygenation
MoS_2
Palm kernel oil
Jet fuel-like hydrocarbon
Heterogeneous catalysis
Advanced biofuel

ABSTRACT

In the current study, palm kernel oil was used as a renewable feedstock for production of jet fuel-like hydrocarbons via the deoxygenation over the Ni-MoS_2/γ-Al_2O_3 catalyst. The dominant C12 fatty acid content in palm kernel oil makes it promising for jet fuel application. Synthesized by a liquid processing method with thiourea organosulfur agent, the catalyst revealed MoS_2 structure with low stacking, while Ni substitution in the MoS_2 structure and interaction with the Al_2O_3 support were determined based on the Ni K-edge XANES and EXAFS results. A high hydrodeoxygenation (HDO) activity, which as the major pathway in the deoxygenation, was observed upon application of a H_2 pressure of 30–50 bar over Ni-MoS_2/γ-Al_2O_3. The optimum product yield of approximately 92% was obtained mainly from the HDO pathway (~60%) with 58% selectivity to C10–C12 jet fuel hydrocarbons. The flow property of the jet fuel-like hydrocarbons was more desirable than those obtained from palm olein oil-derived fuel.

1. Introduction

Biofuels, such as biodiesel, bioethanol, biogas, and bio-oil, have played an important role as renewable energy for transportation and power generation due to the depletion of fossil fuel [1–5]. Deoxygenation, which removes oxygenated components from the reactants in the presence of hydrogen gas through hydrodeoxygenation (HDO) and decarbonylation (DCO) and without hydrogen consumption via decarboxylation (DCO_2), has been used in various applications including bio-hydrogenated diesel (BHD) or green diesel production [6–8] and biomass upgrading into valuable chemicals [9]. The HDO applied in the BHD technology has been proposed as a cleaner and more efficient pathway compared to DCO and DCO_2 due to the lack of carbon loss from reactant conversion to hydrocarbons with the released of water as a by-product. However, DCO and DCO_2 lose one carbon atom to CO and CO_2 gas by-products, respectively, resulting in a liquid product with fewer carbons. The feedstock choices for the production of renewable diesel have been studied using various plant oils containing C16–C18 fatty acids as the main component including palm oil, rapeseed oil, jatropha oil, canola oil, and oil-extract from coffee ground [6,8,10–12]. Furthermore, waste-cooking oil, animal fat, and bio-oil have become potential feedstock candidates [13–16].

The deoxygenation catalysts employ various transition metals, metal sulfides, and metal phosphides on supports [9,11,17–24] (e.g., Al_2O_3, SiO_2, zeolite, and graphite). Co or Ni doped MoS_2 has been known as the state-of-the-art catalysts for HDO and hydrodesulfurization (HDS) because of their excellent catalytic performance and cost-effective application for large-scale production. The additional Ni in MoS_2 modifies the surface of MoS_2 to form a Ni-Mo-S phase which is known as the active site of $NiMoS_2$ catalyst [25]. The Ni or Co has proposed as a promoter to enhance catalytic activity of MoS_2 on a support [26,27]. In addition, metal catalysts on oxide supports (e.g., Ni and Co on SiO_2 or Al_2O_3) are not only selective catalysts for DCO and DCO_2 over HDO [28–30], but also proposed to use for other applications such as Ni-based catalysts in methane reforming [31–33], de-NO_x [34], and oxygen reduction reaction (ORR). [35,36] The catalytic mechanism of Ni-MoS_2 has been studied computationally and experimentally in the unsupported catalyst systems [25,37,38]. The sulfur vacancies in Mo-$36S_2$ have been proposed as the active sites for deoxygenation. The Ni atoms (dopants) favored the substitution into S-edges of MoS_2 structure, creating more sulfur vacancies and leading to enhancement of deoxygenation activity in Ni-MoS_2 with respect to MoS_2. In the system with a carboxylic acid reactant, the Ni promoter at the edge of the MoS_2 demonstrated the synergistic effect

* Corresponding author.
E-mail address: kajornsak@nanotec.or.th (K. Faungnawakij).

http://dx.doi.org/10.1016/j.enconman.2016.12.034
0196-8904/

as the Ni-Mo-S phase which induced smaller activation energies in comparison to those of non-promoted MoS_2 for both the C=O hydrogenation and C—OH bond breaking steps [25]. The catalyst support in Ni-MoS_2 has been shown as the main source of catalyst acidity, i.e. Brønsted acid and/or Lewis acid, leading to isomerization and cracking reactions. The Al_2O_3 support is considered as a weakly-acidic support due to the majority of Al-octahedra in the structure compared with zeolites. Thus, Ni-MoS_2 on alumina support generally showed relatively low tendency of isomerization and cracking activities. Interestingly, the acidity modification of Al_2O_3 support (via Brønsted sites) has been reported as the positive influence on the hydrogenation activity of the MoS_2 and Co-MoS_2 catalysts because of the direct change in their electronic properties [27].

Sulfidation by H_2S, CS_2, and dimethyldisulfide ($C_2H_6S_2$) are common in the synthesis of MoS_2-based catalysts. Nevertheless, the H_2S is a highly toxic gas that is expensive compared to other industrial gases, and therefore, special material-handling equipments are required. In addition, to allow the solid-gas phase reaction to produce a desirable phase, the formation of metal sulfide on the support may require a long preparation period. However, this long period may lead the aggregation of catalyst particles and ultimately a low surface area. Therefore, water-soluble sulfiding agents may promote sulfurization, which is applicable for preparation of supported catalysts and compatible with an impregnation method. Recently, thiourea ($CS(NH_2)_2$) was proposed for synthesis of unsupported MoS_2 catalysts [39–41]. However, MoS_2 on a support material prepared using this method has not been previously reported for the deoxygenation of biofuel. In our study, Ni-MoS_2 on aγ-Al_2O_3 support was prepared using thiourea sulfurization at low temperatures. The cooperation of Ni in the MoS_2 structure and interaction with Al_2O_3 were investigated using the X-ray absorption technique. The deoxygenation activities of the as-synthesized catalysts were studied using palm kernel oil, which is an abundant source of lauric acid (C12), to produce renewable jet fuel-like hydrocarbons. To provide a simple approach for large-scale preparation, sulfidation by thiourea in a liquid-phase processing will be compatible with a general synthesis method of unsupported and supported metal sulfide catalysts. The exploration of a new potential biojet fuel resource via triglyceride-feedstock conversion could provide a straightforward process for obtaining a high yield and tunable biojet fuel via deoxygenation and further isomerization.

2. Experimental

2.1. Catalyst preparation and characterization

The Ni-MoS_2/γ-Al_2O_3 catalyst was prepared by wetness impregnation with a precursor solution based on modification of our previously reported protocol [39] using thiourea as a sulfur agent. A mixture of nickel nitrate hexahydrate ($Ni(NO_3)_2{\cdot}6H_2O$, Sigma-Aldrich, 98.8%), $(NH_4)_6Mo_7O_{24}{\cdot}4H_2O$ (Carlo Erba, 99.0%), and thiourea ($CS(NH_2)_2$, Sigma-Aldrich, 99.0%) was dissolved in water with 1:20 M ratio of molybdenum salt : thiourea. The solution containing a Ni/Ni + Mo ratio of 0.33 was stirred for 0.5–1 h prior to adding sphericalγ-Al_2O_3 (1.8 mm of O.D., Sasol Company) at 85 wt.% of the catalyst followed by stirring at 60 °C for an additional 1–2 h. After impregnation, the sample was dried in an oven for 10–12 h and calcined in an Ar atmosphere for 4 h at 400 °C with a heating rate of 10 °C min^{-1}. The final active phase Ni-MoS_2 was approximately 15 wt.% in the obtained catalyst. The actual molar ratio of Ni/(Ni + Mo) in the calcined catalyst was determined to be approximately 0.32 using inductively coupled plasma-optical emission spectrometry (ICP-OES). Phase identity of the catalyst was analyzed by X-ray diffraction (XRD) using a Bruker D8 Advance with Cu Kα radiation. The measurement was carried out at 40 kV and 40 mA and over a range of $10° < \theta < 80°$ (0.02 deg s^{-1} with a step time of 1 s. The Brunauer–Emmett–Teller (BET) surface area and Barrett-Joyner-Halenda (BJH) pore size of the catalysts were investigated by a N_2 sorption analyzer (Quanta Chrome NOVA2000e). The catalyst morphology was measured using transmission electron microscopy at 200 kV (TEM, TECNAI G2 20 S-Twin). The sample was ground into a fine powder and dispersed in methanol before mounted on a Cu grid coated with a thin film carbon for TEM analysis. The chemical state at the surface of the catalyst was analyzed by X-ray photoelectron spectroscopy (XPS, Kratos AXIS Ultra DLD). In our study, synchrotron-based X-ray absorption spectroscopy (XAS), which is a powerful structure-based technique, has been employed to study the electronic and local structural information of the materials [42]. The XAS spectra including X-ray absorption near edge structure (XANES) and extended X-ray absorption fine structure (EXAFS) spectra were acquired at the SUT-NANOTEC-SLRI XAS Beamline (BL 5.2) (bending magnet; electron energy of 1.2 GeV; beam current of 80–150 mA; 1.1–1.7 × 1011 photon s-1) at the Synchrotron Light Research Institute (SLRI), Nakhon Ratchasima, Thailand. The Mo L3-edge and Ni K-edge spectra were collected in transmission mode using InSb(1 1 1) and Ge (2 2 0) double crystal monochromators with an energy resolution ($\Delta E/E$) of 2×10^{-4}. The background correction and data fitting of the XANES and EXAFS data were done using the ATHENA and ARTEMIS programs in the IFEFFIT package [43,44]. The FTIR analysis was done using KBr pellet preparation method and scanning range from 4000 to 400 cm^{-1}, and the FTIR spectrum of the Ni-MoS_2/γ-Al_2O_3 is shown in Fig. S1 (Supplementary Material).

2.2. Catalytic reaction testing

Refined palm kernel oil and palm olein oil were commercially obtained from a local market in Thailand. As shown in Table 1, the fatty acid contents in the commercial oil were determined through fatty acid methyl esters (FAMEs) obtained by total transesterification of triglycerides at 65 °C for 4 h with methanol (9:1 mol ratio of methanol to oil) using a sodium methoxide ($NaOCH_3$) catalyst (1 wt.% of oil). Acid value of the palm kernel oil was estimated by the titration method with KOH (0.1 M).

The palm olein oil consisted of C12–C20 fatty acids with oleic acid (C18:1) as the major component [45], which is preferred in synthetic diesel fuel production. The refined palm kernel oil (acid value of 0.26 mg KOH/g of oil) contained a high component of lauric acid (C12:0), which is suitable for biojet fuel application. The catalytic deoxygenation reactions were performed in a custom-made trickle-bed reactor with an internal diameter of 0.7 cm, length of 21 cm, and volume of 8.1 cm^3. After NiMoS_2/Al_2O_3

Table 1
Fatty acid content of commercial refined palm kernel oil compared to that of palm olein oil.

Fatty acid	Composition (wt.%)	
	Palm olein oil	Palm kernel oil
C8:0	–	1.2
C10:0	–	2.6
C12:0	0.4	48.8
C14:0	0.8	17.3
C16:0	37.4	–
C16:1	0.2	9.1
C18:0	3.6	2.1
C18:1	45.8	16.1
C18:2	11.1	2.3
C18:3	0.3	0.1
C20:0	0.3	–
C20:1	0.1	0.1

loading in the reactor, the system was pressurized with H_2 to the desired pressure and heated to the desired reaction temperature. The oil feeds were introduced to the reactor by a HPLC pump, and H_2 feed was controlled by mass flow controllers. The deoxygenation reactions were tested using the following conditions: reaction temperature of 270–330 °C, H_2 pressure of 30–50 bars, liquid hourly space velocity (LHSV) of 1–5 h^{-1}, and H_2/oil ratio of 1000 N(cm^3°cm^{-3}). Each reaction parameter was evaluated using fresh catalyst to eliminate the effect of catalyst deactivation during the experiments. The three experiments using the same catalyst were performed and the liquid product was collected every 3 h interval for analysis. Thus, typically the total time on stream on each reaction condition was 9 h while the catalytic activity remained stable.

Gas chromatograph instruments were used to identify the obtained products. A GC-2014 Shimadzu and a GC–MS Agilent 7890A equipped with DB-1HT (30 m × 0.32 mm × 0.1 μm) capillary columns were used for liquid product analysis. The calibration curve of standards was used to quantify a composition of n-alkanes in liquid products. In details, a diluted sample was injected into the GC with the split ratio of 100. An injection temperature of 340 °C, a detector temperature of 370 °C and a column temperature ramping from 40 to 270 °C) were used for the analysis. An online Shimadzu GC-14B equipped with molecular sieve 5A and Porapak Q packed columns was used for gas product analysis. The deoxygenation activities were calculated as shown in the following equations.

$$\textit{Triglycerides conversion}\ (\%) = \frac{\textit{mole of triglycerides in feed-mole of triglycerides in product (mole)}}{\textit{mole of triglycerides in feed (mole)}} \times 100\% \quad (1)$$

$$\textit{Liquid product yield}\ (\%) = \frac{\textit{total mole of n-alkanes in liquid product}}{\textit{total mole of fatty acids in feed}} \times 100\% \quad (2)$$

$$\textit{HDO selectivity}\ (\%) = \frac{\textit{total mole of n-alkanes (C8, C10, C12, C14, C16, C18) in liquid product}}{\textit{total mole of fatty acids in feed}} \times 100\% \quad (3)$$

$$\textit{DCO} + \textit{DCO2 selectivity}\ (\%) = \frac{\textit{total mole of n-alkanes (C7, C9, C11, C13, C15, C17) in liquid product}}{\textit{total mole of fatty acids in feed}} \times 100\% \quad (4)$$

$$\textit{C10 to C12 selectivity}\ (\%) = \frac{\textit{total mole of n-alkanes (C10, C11, C12) in liquid product}}{\textit{total mole of fatty acids in feed}} \times 100\% \quad (5)$$

The heating values of the liquid products were also via a bomb calorimeter (LECO AC350), and the flow property was determined using automated cloud point and pour point analyzers (ISL CPP 5GS).

3. Results and discussion

As shown in Fig. 1, the XRD pattern of a calcined Ni-MoS_2/γ-Al_2O_3 sample that was prepared using our new method with

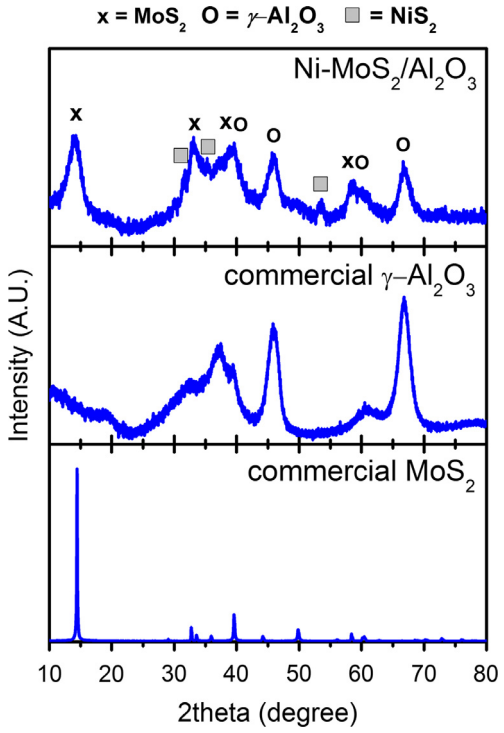

Fig. 1. XRD patterns of Ni-doped MoS_2/Al_2O_3 compared to those of commercialγ-Al_2O_3 and commercial MoS_2.

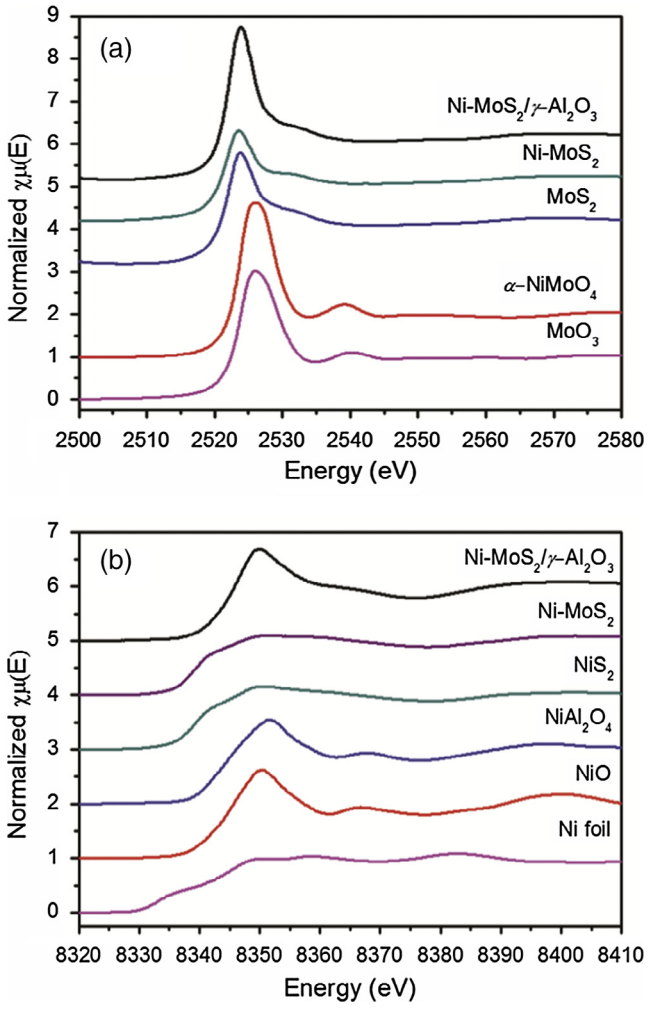

Fig. 2. (a) XANES spectra at Mo L_3-edges of Ni-MoS_2/γ-Al_2O_3 compared to those of Mo compounds and (b) XANES spectra at Ni K-edges of Ni-MoS_2/Al_2O_3 compared to those of Ni compounds.

thiourea as a sulfiding agent indicated that the bulk phases of the catalysts on theγ-Al_2O_3 support included NiS_2 (PDF 03-065-3325), and MoS_2 corresponding to PDF 03-065-0160 as well as commercial MoS_2 (Sigma-Aldrich). The peak broadening shown in the XRD pattern of the catalyst was due to the semi-amorphous nature and small crystallite size (i.e., 5–10 nm determined by Scherrer's equation). Additionally, the broad MoS_2 peaks may indicate the low stacking and disorder of the MoS_2 layers [46].

In addition, the Mo and Ni oxidation state and crystallinity of the bulk Ni-MoS_2/γ-Al_2O_3 material were confirmed by the XANES spectra [47] at Mo L_3-edges and Ni K-edges (Fig. 2). As shown in Fig. 2(a), the Mo L_3-edge positions of Mo(0) (standard Mo metal foil, 2520.0 eV), Mo(IV) (MoS_2, 2522.3 eV) and Mo(VI) (MoO_3, α-$NiMoO_4$, 2524.1 eV) increased with the ionicity of the Mo bonding and electronegativity of the anions. The near-edge and post-edge features of the MoS_2-based compounds exhibited less intense amplitudes (low-k scattering), indicating poor crystallinity in the amorphous phase. Moreover, as seen in Fig. 2(a), the white line intensity of Ni-MoS_2 became smaller and that of Ni-MoS_2/Al_2O_3 turned into higher when compared with that of MoS_2 standard, suggesting an existence of Ni-substitution in both samples. Besides, the Ni K-edge XANES spectra of Ni-MoS_2/γ-Al_2O_3 compared to those of some Ni compounds indicated that the edge energy (at 8345.6 eV) was between those of the $NiAl_2O_4$ (8346.1 eV), NiO (8345.9 eV), and NiS_2 (8339.4 eV) standards, as shown in Fig. 2(b). These results confirmed the presence of both Ni-S and Ni-O bonds, which may arise at the metal-support interface between Ni and MoS_2 and alumina, respectively. Based on the different post-edge features, unlike those in NiO and NiS_2 standards, this result also suggested the substitution of Ni into the MoS_2 and MoS_2/Al_2O_3 structures which is consistent with the observed Mo L3-edge XANES results. In order to clarify the Ni-substitution in samples, the EXAFS data at Ni K-edge is necessarily employed. The measured EXAFS spectra (black line) and the best fitting (red line) at Ni K-edge for the Ni-MoS_2 and Ni-MoS_2/Al_2O_3 samples are shown in Fig. 3 (in real space), and the fitting parameters are listed in Table 2. The mean Ni-S and Ni-S/Ni-O coordination numbers and bonding distances around the Ni atoms in the MoS_2 and MoS_2/Al_2O_3 samples were 4.78(2) and 1.68(1)/3.40(2) and 2.223(4) Å and 2.204(1)/2.025(3) Å, respectively. These EXAFS results confirmed Ni substitution into the MoS_2 and MoS_2/Al_2O_3 structures, which is consistent with the reported XANES results. The metal doping in the based catalysts, i.e. Ni or Co doping in MoS_2 [39,48], Co doping in lattices of MoO_2 [22], has been confirmed as the promoting effect to improve catalytic deoxygenation performance by modification of the electronic and geometric surface structure of the catalytic active sites via defects [48] e.g. S-vacancies in MoS_2.

Table 2
Ni K-edge EXAFS fitting parameter of Ni-MoS_2/γ-Al_2O_3 prepared by thiourea sulfurization.

Samples	Paths	Coordination number (N)	σ^2	ΔE (eV)	R (Å)
Ni-MoS_2	Ni-S	4.78(2)	0.002	−6.916	2.223(4)
Ni-MoS_2/Al_2O_3	Ni-S	1.68(1)	0.005	−4.515	2.204(1)
	Ni-O	3.40(2)	0.007	−4.095	2.025(3)

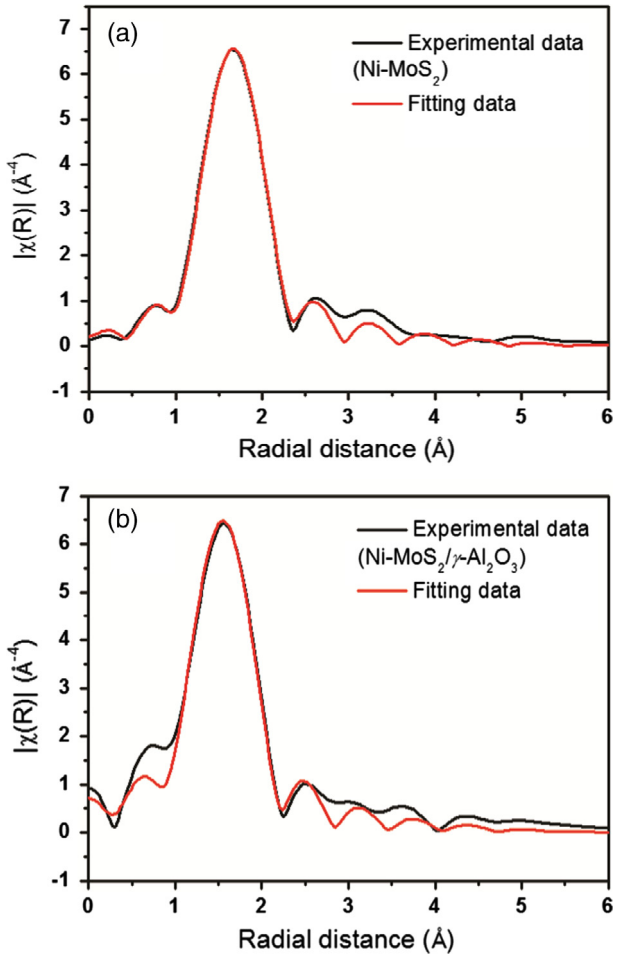

Fig. 3. Measured EXAFS data with the best fitting at the Ni K-edge for the Ni-MoS_2 and Ni-MoS_2/γ-Al_2O_3 samples.

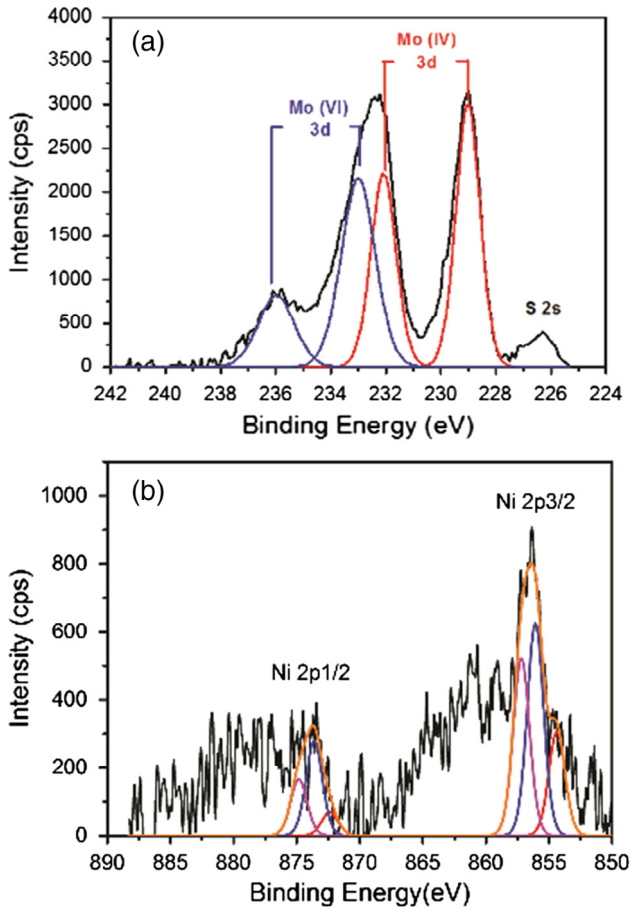

Fig. 4. XPS spectra of Ni-doped MoS_2/Al_2O_3: (a) Mo 3d and S 2s region and (b) Ni 2p region.

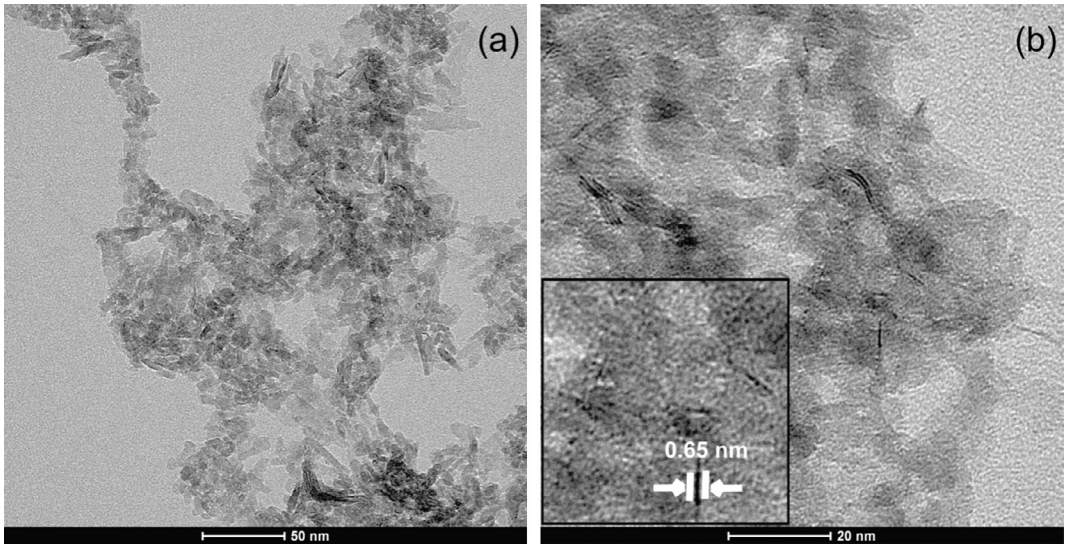

Fig. 5. TEM images of Ni-MoS_2/γ-Al_2O_3: (a) low magnification and (b) high magnification.

Table 3
Surface area and porous parameters of prepared catalysts.

Catalysts	S_{BET} ($m^2\ g^{-1}$)	Average BJH pore volume ($cm^3\ g^{-1}$)	Average BJH pore diameter (nm)
γ-Al_2O_3	181	0.510	7.5
Ni-MoS_2/γ-Al_2O_3	156	0.306	7.0

However, the chemical state of the catalyst surface measured using the XPS technique (Fig. 4a) indicate the presence of at least two Mo species on the surface of the catalyst that exist as a mixture of Mo(IV) from MoS_2 and Mo(VI), which may arise from MoO_3 due to the formation of an oxide layer at the surface in contact with Al_2O_3. The peaks for Mo 3d5/2 at 229.0 eV and Mo3d3/2 at 232.1 eV were assigned to Mo(IV) in MoS_2, and the peaks for Mo3d3/2 at 232.9 eV and Mo 3d3/2 at 236.0 eV were assigned to

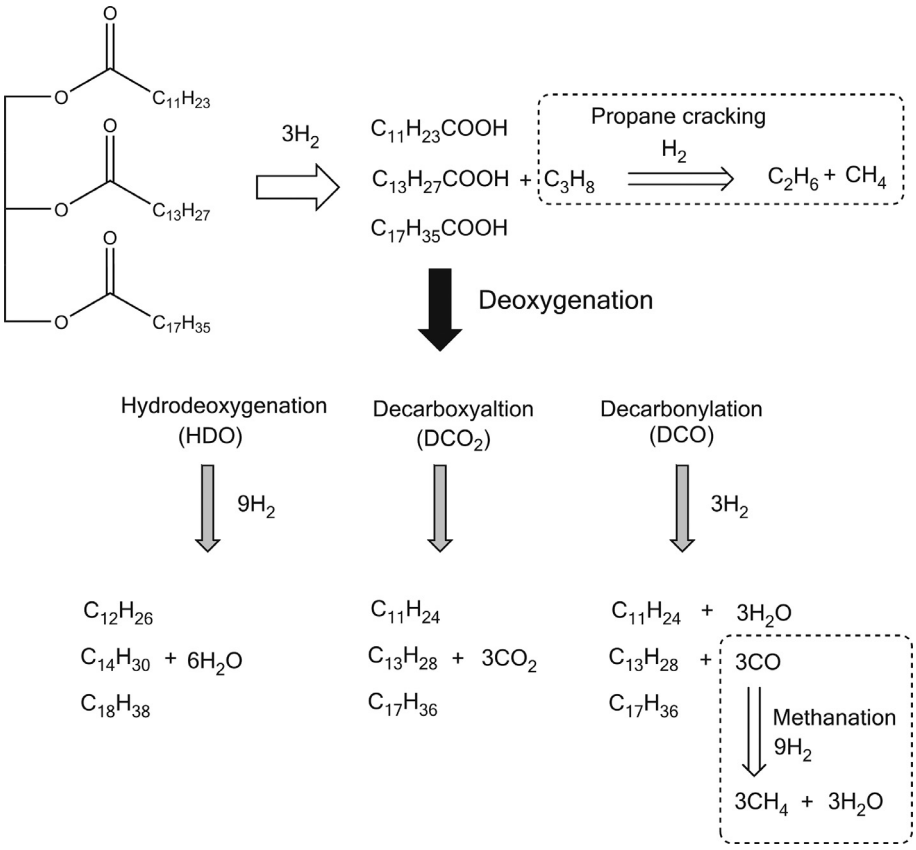

Scheme 1. Proposed catalytic palm kernel oil conversion via deoxygenation into jet diesel-like hydrocarbons.

Mo(VI) in MoO_3 [49,50]. The presence of Ni (II) based on the XPS spectrum of Ni 2p was confirmed, as shown in Fig. 4b. The Ni 2p bands, the doublet 2p3/2 and 2p1/2 due to spin-orbit splitting, were fitted to the 3 species of Ni(II). The binding energy of Ni 2p3/2 around 854.6 eV could be related to the nickel sulfide compound (854–855 eV); this would be assigned for the NiS_2 in this case. The binding energy around 855.9 eV corresponded to Ni in $NiMoS_2/Al_2O_3$ [51] and the BE around 857.3 eV was close to either the Ni species in the interaction with the alumina support at the metal-support interface [52]. The broad bands around 860–865 eV and 878–885 eV were ascribable to the shake-up satellites structure of Ni(II) [51].

The layered structure of MoS_2 was observed in the TEM images (Fig. 5) as the dark line stacking, which represents a d(002) distance of 0.65 nm for crystalline MoS_2. This result is similar to the theoretical distance (0.62 nm), as shown in Fig. 5(b). The number of layers was random and ranged from 1 to 4 layers (average of 1.8 layers), which is considered to be low stacking due to the low temperature synthesis [53]. The size of the MoS_2 sheets, which is the length of the dark lines, ranged from 2 to 9 nm (average of 4.1 nm), and the crystals of γ-Al_2O_3 support were approximately 5–20 nm in size. It should be noted that the particle size of the supported catalyst observed via an SEM technique was in a range of 0.5–5 μm, suggesting the agglomeration forms of the catalyst particles (results not shown). As shown in Table 3, the specific surface area of Ni-MoS_2/γ-Al_2O_3 synthesized using our method exhibited a slightly lower surface area, pore volume, and average pore size compared to that of γ-Al_2O_3 due to the deposition of Ni-MoS_2 on the surface and possibly inside the pores of the alumina.

The deoxygenation of palm kernel oil using Ni-MoS_2/γ-Al_2O_3 under an excess H_2 atmosphere was performed with a custom-made trickle-based reactor. The proposed reaction pathways, represented in Scheme 1, were similar to those reported in different triglyceride feedstock [54,55]. The triglycerides in palm kernel oil were degraded to propane gas and fatty acid molecules that consisted of primarily C12 with some C14 and C18, as shown in the Table 1. The deoxygenation of these fatty acids to obtain a biofuel product was proposed to occur via three main reactions. Hydrodeoxygenation (HDO), which is the primary H_2 consumption pathway, produced alkanes with the same number of carbon atoms as well as water as a by-product via C—O bond cleavage. Decarbonylation (DCO), which used the least H_2, and decarboxylation (DCO_2), which does not use H_2, produced alkanes via C—C bond cleavage leading to the loss of one carbon atom to CO gas and water (DCO) and CO_2 gas (DCO_2), respectively.

As shown in Fig. 6a, an increase in the reaction temperature under a H_2 pressure of 50 bar and LHSV of 1 h^{-1} enhanced the yield due to improvement in the product yield via DCO_2 and DCO reactions. However, the selectivity to the HDO product was slightly higher when comparing those at 270 °C and 300 °C and slightly lower at 330 °C, and the selectivity of the competitive DCO_2 + DCO

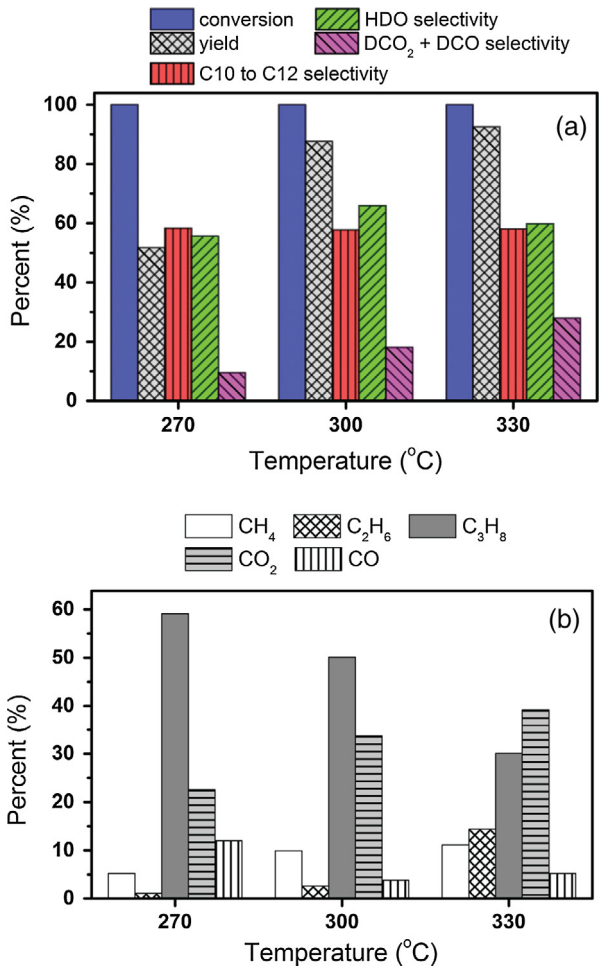

Fig. 6. Effect of reaction temperature on deoxygenation of palm kernel oil under a H_2 pressure of 50 bar and LHSV of 1 h^{-1}: (a) catalytic performance based on liquid product and (b) gas product distribution (%mol).

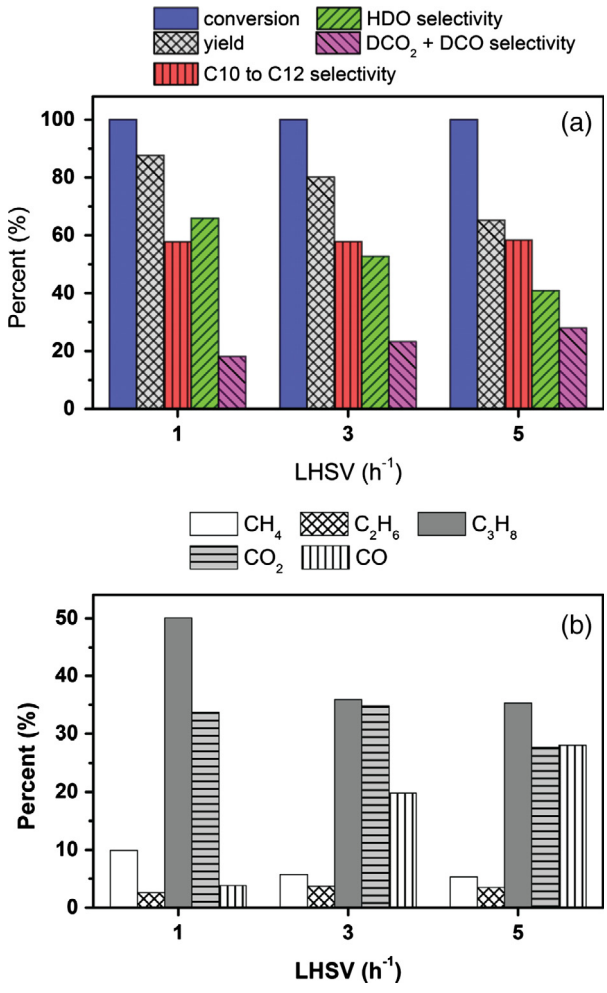

Fig. 7. Effect of LHSV on deoxygenation of palm kernel oil at 300 °C and a H_2 pressure of 50 bar: (a) catalytic performance based on liquid product and (b) gas product distribution (%mol).

reactions increased based on gas product distribution (Fig. 6b). These results are in good agreement with the exothermic nature of HDO [56], which is unfavorable at higher temperature. Nevertheless, the HDO pathway still dominated the total reactions at 270–330 °C. Cracking as a side reaction tended to occur at high temperatures, especially propane cracking at 330 °C based on an increase in the ethane composition in the gas product. Moreover, methanation (i.e., CO conversion to CH_4) may occur starting at 300 °C due to a decrease in CO, which was inversely proportional to CO_2 accumulation. It should be noted that the C10–C12 selectivity in the liquid product remained almost constant at all reaction temperatures. In the study of the LHSV parameter, a shorter contact time between the reactant and the catalyst (high LHSV) led to a significant decrease in the HDO product contribution and a small increase in the DCO_2 + DCO product contribution, which resulted in a decrease in the total yield (Fig. 7a). Moreover, the CO distribution in the gas product increased at a high LHSV, indicating that the DCO pathway is favored at a short resident time (Fig. 7b). As the H_2 pressure increased (Fig. 8a), the liquid yield increased as a result of the domination of the HDO activity under the H_2 rich conditions at the catalyst surface over those from the DCO_2 + DCO pathways due to the large H_2 consumption required in the HDO pathway [10,54]. The CO amount in the gas product was suppressed at H_2 pressure of 50 bar, and the CO_2 level remained similar to that at lower H_2 pressures (Fig. 8b). It is important to note that methanation, which is favorable under high H_2 pressure conditions [57], may have occurred at a H_2 pressure of 50 bar based on the slight increase in the methane amount compared to that of ethane. The turnover frequency (TOF), a generation rate of liquid product per the active site determined by CO uptake on the catalyst surface, was 0.0260 s^{-1} for the condition of 330 °C, H_2 pressure of 5 MPa, and LHSV of 1 h^{-1}.

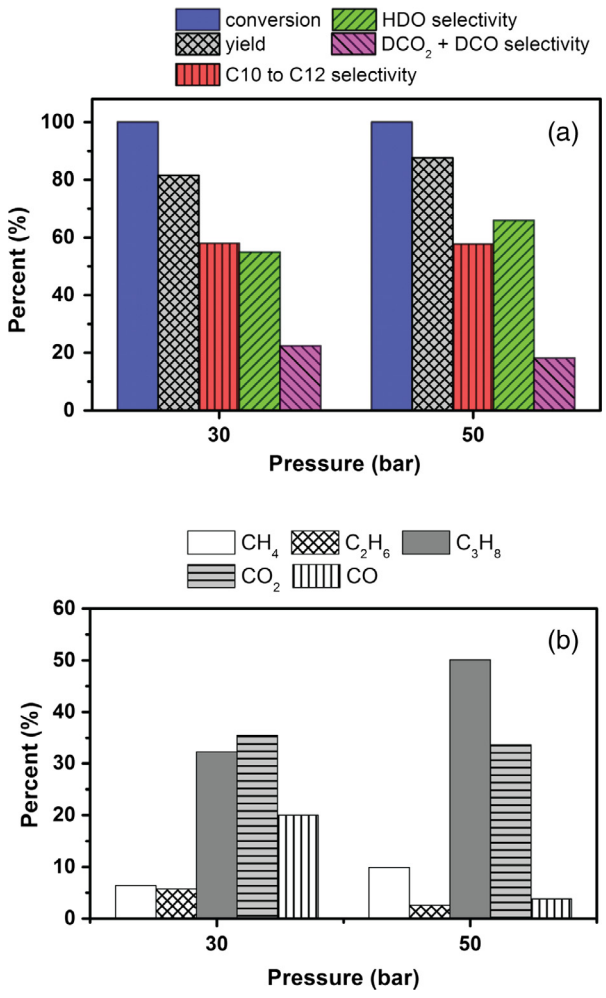

Fig. 8. Effect of H_2 pressure on deoxygenation of palm kernel oil at 300 °C and a LHSV of 1 h^{-1}: (a) catalytic performance based on liquid product and (b) gas product distribution (%mol).

To clarify the role of each catalyst phase, the deoxygenation experiments were carried out over Ni/γ-Al_2O_3, NiS_2/γ-Al_2O_3, MoS_2/γ-Al_2O_3, and Ni-MoS_2/γ-Al_2O_3 as the results shown in Table S1 (Supplementary Material). The low reaction temperature of 240 °C was intentionally used to keep the product yield in the range below 15%. The conversion of triglyceride was obtained in the range of 89–95% over all catalysts, while Ni-MoS_2/γ-Al_2O_3 gave the highest conversion. This result suggested that triglyceride can be easily converted even at such low temperature. Ni/γ-Al_2O_3 and NiS_2/γ-Al_2O_3 provided extremely low liquid yield of 0.7 and 1.2%, respectively. Compared with the activity of Ni/γ-Al_2O_3 and NiS_2/γ-Al_2O_3, MoS_2/γ-Al_2O_3 gave significantly higher yield of 9.0% with HDO selectivity of 5.5% and DCO + DCO_2 selectivity of 2.9%. Interestingly, along with the highest triglyceride conversion, the highest liquid yield of 11.8% was achieved over Ni-MoS_2/γ-Al_2O_3 catalyst. Doping Ni species to MoS_2 structure clearly enhanced HDO selectivity. The result confirmed the Ni substitution in Ni-MoS_2 catalyst system and was in line with the X-ray analyses. The Ni-substituted MoS_2 and MoS_2 were considered to be a main active phase for the deoxygenation process of palm kernel oil. It should be noted that the phase identity of the used Ni-MoS_2/γ-Al_2O_3 catalyst, investigated by XRD (Fig. S2), was similar to that of the fresh catalyst with an additional Ni metal phase (PDF 00-004-0850) due to partial reduction of Ni species under deoxygenation condition in high H_2 pressure.

The conversion of palm kernel oil was >99% under various operational conditions in the current study (i.e., reaction temperature, LHSV, and H_2 pressure). Therefore, the selectivity to C10–C12 alkanes in the liquid product remained at approximately 58%, corresponding to the amount of lauric acid in the palm kernel oil feedstock. In addition, the catalytic activities of the different oil feedstocks (i.e., palm kernel oil and palm olein oil) based on the yield contributed by the high HDO product selectivity were similar (result not shown). Therefore, the fatty acid chain did not significantly affect the deoxygenation performance over the Ni-MoS_2/γ-Al_2O_3 catalyst under the studied conditions. Depending on the product composition, the liquid biofuel from palm kernel oil consisted of jet fuel-like hydrocarbons, and product from palm olein oil consisted of diesel-like hydrocarbons. The differences in heating value and cold flow property of biofuel products from the two feedstocks were in association with the composition of the alkanes based on their fatty acid origins, as shown in Table 4. The medium chain alkanes (i.e., C10–C12) in the product obtained from palm kernel oil improved the cloud point (6.2 °C) and pour point (−3.0 °C) while maintaining an excellent high heating value of 46.6 MJ kg^{-1} comparable to the green diesel from palm olein. Typically, the commercial jet fuels contain additives to keep low freezing point, cloud point and pour point, leading to excellent cold flow properties at actual working conditions as seen in Table 4. The fuel property and chemical composition of the additive-free jet fuel-like hydrocarbons in this work could be suitable for blending with fossil jet or diesel range fuel. The isomerization of the developed fuel can also be applicable to improve its cold flow property. In addition, the Ni-MoS_2/γ-Al_2O_3 catalyst prepared by the thiourea solution process demonstrated comparable catalytic deoxygenation performance to those of conventional prepared catalysts in a continuous flow reactor system, as shown in Table 5.

Table 4
Heating values and cold flow properties of liquid products obtained from palm kernel oil, palm olein oil, and commercial jet fuels.

Feedstock	Higher heating value (MJ kg^{-1})	Cloud point (°C)	Pour point (°C)	Remark
Palm kernel oil	46.6	6.2	−3.0	The present work
Palm olein oil	46.0	22.1	19.0	The present work
POSF- 2827 (Jet A type) [58]	n/a	−48.0	−52.5	Commercial Jet fuel, with additives
Jet A-1 type [59]	43.5	−52	n/a	Commercial Jet fuel, with additives

Table 5
Deoxygenation activity comparison in a continuous flow reactor system by using Ni-MoS_2/γ-Al_2O_3 catalysts with different synthesis methods.

Synthesis method	Feedstock	Operating condition	Conversion (%)	Yield (%)	Ref.
Sulfidation via thiourea solution processing	Refined palm kernel oil	330 °C, 5 MPa of H_2, 1 h^{-1} of LHSV	100	~92%	This work
	Refined palm oil	330 °C, 5 MPa of H_2, 1 h^{-1} of LHSV	100	~98	
Conventional in-situ sulfidation in a reactor by CS_2	Refined palm oil	330 °C, 5 MPa of H_2, 1 h^{-1} of LHSV	100	~89%	Srifa et al. [6]
Conventional in-situ sulfidation in a reactor by dimethyl disulfide	Food grade rapeseed oil	280 °C, 3.5 MPa of H_2, 0.25–4 h of contact time (V/F)	80–100	>90%	Kubička and Kaluža [54]
Commercial NiMo/γ-Al_2O_3 and conventional in-situ sulfidation in a reactor by dimethyl disulfide	Waste cooking oil (mainly sunflower oil)	350–390 °C, 1.37 MPa of H_2, 0.5–2.5 h^{-1} of LHSV	>95%	73–82%	Bezergianni et al. [60]
Commercial NiMo/γ-Al_2O_3 (Haldor Topsøe 217) and conventional in-situ sulfidation in a reactor by dimethyl disulfide	Crude palm oil	350 °C, 4–9 MPa of H_2, 2 h^{-1} of LHSV (pilot scale)	100	~100%	Guzman et al. [61]

4. Conclusions

A novel method for metal sulfide preparation using thiourea sulfurization under an inert atmosphere was successfully applied for the synthesis of the Ni-MoS_2/γ-Al_2O_3 catalyst. The catalytic performance for the deoxygenation of palm kernel oil was studied as an alternative approach for the production of jet fuel-like hydrocarbons. A high HDO activity, which was the major pathway for deoxygenation, was observed a high H_2 pressure was applied at 300 °C with a long contact time (low LHSV) between the reactants and the catalyst. The promotion of DCO_2 and DCO occurred as the reaction temperature increased and with a short resident time (fast LHSV). The side reactions, such as cracking and methanation, occurred at high temperatures, such as 330 °C. The optimum product yield was approximately 92%, which was primarily from the HDO product (~60%) with 58% selectivity to C10–C12 for the jet fuel-like hydrocarbons under the following conditions: 330 °C, H_2 pressure of 50 bar, LHSV of 1 h^{-1}, and H_2/oil ratio of 1000 N (cm^3 cm^{-3}).

Acknowledgments

This work was supported by the National Nanotechnology Center (NANOTEC) under National Science and Technology Development Agency (NSTDA) and the Thailand Research Fund (TRF), Thailand under contract no. TRG5880192 and RSA5580055. The XAS and XPS experiments were performed at the BL-5.2 SUT-NANOTEC-SLRI XAS Beamline and the SUT-NANOTEC-SLRI XPS, respectively.

Appendix A. Supplementary material

Supplementary data associated with this article can be found, in the online version, at http://dx.doi.org/10.1016/j.enconman.2016.12.034.

References

[1] Demirbaş A. Biomass resource facilities and biomass conversion processing for fuels and chemicals. Energy Convers Manage 2001;42:1357–78.
[2] Chheda JN, Huber GW, Dumesic JA. Liquid-phase catalytic processing of biomass-derived oxygenated hydrocarbons to fuels and chemicals. Angew Chem Int Ed Engl 2007;46:7164–83.
[3] dos Santos TR, Harnisch F, Nilges P, Schröder U. Electrochemistry for biofuel generation: transformation of fatty acids and triglycerides to diesel-like olefin/ether mixtures and olefins. ChemSusChem 2015;8:886–93.
[4] Mansir N, Taufiq-Yap YH, Rashid U, Lokman IM. Investigation of heterogeneous solid acid catalyst performance on low grade feedstocks for biodiesel production: a review. Energy Convers Manage 2016. http://dx.doi.org/10.1016/j.enconman.2016.07.037.
[5] Soltani S, Rashid U, Al-Resayes SI, Nehdi IA. Recent progress in synthesis and surface functionalization of mesoporous acidic heterogeneous catalysts for esterification of free fatty acid feedstocks: a review. Energy Convers Manage 2016. http://dx.doi.org/10.1016/j.enconman.2016.07.042.
[6] Srifa A, Faungnawakij K, Itthibenchapong V, Viriya-Empikul N, Charinpanitkul T, Assabumrungrat S. Production of bio-hydrogenated diesel by catalytic hydrotreating of palm oil over $NiMoS_2$/γ-Al_2O_3 catalyst. Bioresour Technol 2014;158:81–90.
[7] Han J, Duan J, Chen P, Lou H, Zheng X, Hong H. Carbon-supported molybdenum carbide catalysts for the conversion of vegetable oils. ChemSusChem 2012;5:727–33.
[8] Phimsen S, Kiatkittipong W, Yamada H, Tagawa T, Kiatkittipong K, Laosiripojana N, et al. Oil extracted from spent coffee grounds for bio-hydrotreated diesel production. Energy Convers Manage 2016;126:1028–36.
[9] Alonso DM, Wettstein SG, Dumesic JA. Bimetallic catalysts for upgrading of biomass to fuels and chemicals. Chem Soc Rev 2012;41:8075–98.
[10] Liu Y, Sotelo-Boyás R, Murata K, Minowa T, Sakanishi K. Hydrotreatment of vegetable oils to produce bio-hydrogenated diesel and liquefied petroleum gas fuel over catalysts containing sulfided Ni–Mo and solid acids. Energy Fuels 2011;25:4675–85.
[11] Wang C, Tian Z, Wang L, Xu R, Liu Q, Qu W, et al. One-step hydrotreatment of vegetable oil to produce high quality diesel-range alkanes. ChemSusChem 2012;5:1974–83.
[12] Kubička D, Horáček J. Deactivation of HDS catalysts in deoxygenation of vegetable oils. Appl Catal, A 2011;394:9–17.
[13] Toba M, Abe Y, Kuramochi H, Osako M, Mochizuki T, Yoshimura Y. Hydrodeoxygenation of waste vegetable oil over sulfide catalysts. Catal Today 2011;164:533–7.
[14] Bezergianni S, Kalogianni A, Dimitriadis A. Catalyst evaluation for waste cooking oil hydroprocessing. Fuel 2012;93:638–41.
[15] Kaewmeesri R, Srifa A, Itthibenchapong V, Faungnawakij K. Deoxygenation of waste chicken fats to green diesel over Ni/Al_2O_3: effect of water and free fatty acid content. Energy Fuels 2015. 150116163647003.
[16] Puértolas B, Keller TC, Mitchell S, Pérez-Ramírez J. Deoxygenation of bio-oil over solid base catalysts: from model to realistic feeds. Appl Catal, B 2016;184:77–86.
[17] Popov A, Kondratieva E, Goupil JM, Mariey L, Bazin P, Gilson J-P, et al. Bio-oils hydrodeoxygenation: adsorption of phenolic molecules on oxidic catalyst supports. J Phys Chem C 2010;114:15661–70.
[18] Wu S-K, Lai P-C, Lin Y-C, Wan H-P, Lee H-T, Chang Y-H. Atmospheric hydrodeoxygenation of guaiacol over alumina-, zirconia-, and silica-supported nickel phosphide catalysts. ACS Sus Chem Eng 2013;1:349–58.
[19] Teerawit Prasomsri TN, Román-Leshkov Yuriy. Effective hydrodeoxygenation of biomass-derived oxygenates into unsaturated hydrocarbons by MoO_3 using low H_2 pressures. Energy Environ Sci 2013;6:1732–8.
[20] Chen L, Fu J, Yang L, Chen Z, Yuan Z, Lv P. Catalytic hydrotreatment of fatty acid methyl esters to diesel-like alkanes over Hβ zeolite-supported nickel catalysts. ChemCatChem 2014;6:3482–92.

[21] Yeh T, Linic S, Savage PE. Deactivation of Pt catalysts during hydrothermal decarboxylation of butyric acid. ACS Sus Chem Eng 2014;2:2399–406.
[22] Ding R, Wu Y, Chen Y, Chen H, Wang J, Shi Y, et al. Catalytic hydrodeoxygenation of palmitic acid over a bifunctional Co-doped MoO_2/CNTs catalyst: an insight into the promoting effect of cobalt. Catal Sci Tech 2016.
[23] Silva LN, Fortes ICP, de Sousa FP, Pasa VMD. Biokerosene and green diesel from macauba oils via catalytic deoxygenation over Pd/C. Fuel 2016;164:329–38.
[24] Al-Muhtaseb AaH, Jamil F, Al-Haj L, Al-Hinai MA, Baawain M, Myint MTZ, et al. Efficient utilization of waste date pits for the synthesis of green diesel and jet fuel fractions. Energy Convers Manage 2016;127:226–32.
[25] Ruinart de Brimont M, Dupont C, Daudin A, Geantet C, Raybaud P. Deoxygenation mechanisms on Ni-promoted MoS_2 bulk catalysts: a combined experimental and theoretical study. J Catal 2012;286:153–64.
[26] Okamoto Y, Hioka K, Arakawa K, Fujikawa T, Ebihara T, Kubota T. Effect of sulfidation atmosphere on the hydrodesulfurization activity of SiO_2-supported Co–Mo sulfide catalysts: local structure and intrinsic activity of the active sites. J Catal 2009;268:49–59.
[27] Chen W, Maugé F, van Gestel J, Nie H, Li D, Long X. Effect of modification of the alumina acidity on the properties of supported Mo and CoMo sulfide catalysts. J Catal 2013;304:47–62.
[28] Kim SK, Brand S, Lee Hs, Kim Y, Kim J. Production of renewable diesel by hydrotreatment of soybean oil: effect of reaction parameters. Chem Eng J 2013;228:114–23.
[29] Srifa A, Viriya-empikul N, Assabumrungrat S, Faungnawakij K. Catalytic behaviors of Ni/γ-Al_2O_3 and Co/γ-Al_2O_3 during the hydrodeoxygenation of palm oil. Catal Sci Tech 2015;5:3693–705.
[30] Li G, Zhang F, Chen L, Zhang C, Huang H, Li X. Highly selective hydrodecarbonylation of oleic acid into n-heptadecane over a supported nickel/zinc oxide–alumina catalyst. ChemCatChem 2015;7:2646–53.
[31] Zhao X, Li H, Zhang J, Shi L, Zhang D. Design and synthesis of NiCe@m-SiO_2 yolk-shell framework catalysts with improved coke- and sintering-resistance in dry reforming of methane. Int J Hydrogen Energy 2016;41:2447–56.
[32] Xie T, Shi L, Zhang J, Zhang D. Immobilizing Ni nanoparticles to mesoporous silica with size and location control via a polyol-assisted route for coking- and sintering-resistant dry reforming of methane. Chem Commun (Camb) 2014;50:7250–3.
[33] Cao Y, Li H, Zhang J, Shi L, Zhang D. Promotional effects of rare earth elements (Sc, Y, Ce, and Pr) on NiMgAl catalysts for dry reforming of methane. RSC Adv 2016;6:112215–25.
[34] Cai S, Zhang D, Shi L, Xu J, Zhang L, Huang L, et al. Porous Ni-Mn oxide nanosheets in situ formed on nickel foam as 3D hierarchical monolith de-NO_x catalysts. Nanoscale 2014;6:7346–53.
[35] Kariuki NN, Cansizoglu MF, Begum M, Yurukcu M, Yurtsever FM, Karabacak T, et al. SAD–GLAD Pt–Ni@Ni nanorods as highly active oxygen reduction reaction electrocatalysts. ACS Catal 2016;6:3478–85.
[36] Li B, Zhang L, Chen L, Cai X, Lai L, Wang Z, et al. Graphene-supported non-precious metal electrocatalysts for oxygen reduction reactions: the active center and catalytic mechanism. J Mater Chem A 2016;4:7148–54.
[37] Kibsgaard J, Tuxen A, Knudsen KG, Brorson M, Topsøe H, Lægsgaard E, et al. Comparative atomic-scale analysis of promotional effects by late 3d-transition metals in MoS_2 hydrotreating catalysts. J Catal 2010;272:195–203.
[38] Zhang H, Lin H, Zheng Y. The role of cobalt and nickel in deoxygenation of vegetable oils. Appl Catal, B 2014;160–161:415–22.
[39] Itthibenchapong V, Ratanatawanate C, Oura M, Faungnawakij K. A facile and low-cost synthesis of MoS_2 for hydrodeoxygenation of phenol. Catal Commun 2015;68:31–5.
[40] Wang W, Li L, Wu K, Zhu G, Tan S, Li W, et al. Hydrothermal synthesis of bimodal mesoporous MoS_2 nanosheets and their hydrodeoxygenation properties. RSC Adv 2015;5:61799–807.
[41] Liu N, Guo Y, Yang X, Lin H, Yang L, Shi Z, et al. Microwave-assisted reactant-protecting strategy toward efficient MoS_2 electrocatalysts in hydrogen evolution reaction. ACS Appl Mater Interfaces 2015;7:23741–9.
[42] Rehr JJ, Albers RC. Theoretical approaches to x-ray absorption fine structure. Rev Mod Phys 2000;72:621–54.
[43] Newville M. EXAFS analysis using FEFF and FEFFIT. J Synchrotron Radiat 2001;8:96–100.
[44] Ravel B, Newville M. ATHENA, ARTEMIS, HEPHAESTUS: data analysis for X-ray absorption spectroscopy using IFEFFIT. J Synchrotron Radiat 2005;12:537–41.
[45] Viriya-Empikul N, Krasae P, Puttasawat B, Yoosuk B, Chollacoop N, Faungnawakij K. Waste shells of mollusk and egg as biodiesel production catalysts. Bioresour Technol 2010;101:3765–7.
[46] Chianelli RRP, Prestridge EB, Pecoraro TA, Deneufville JP. Molybdenum disulfide in the poorly crystalline "Rag" structure. Science 1979;203:1105–7.
[47] Surisetty VR, Hu Y, Dalai AK, Kozinski J. Structural characterization and catalytic performance of alkali (K) and metal (Co and Rh)-promoted MoS_2 catalysts for higher alcohols synthesis. Appl Catal, A 2011;392:166–72.
[48] Lauritsena Jeppe V, Kibsgaard J, Olesena Georg H, Moses Poul G, Hinnemann Berit, Helveg Stig, et al. Flemming Besenbacher Location and coordination of promoter atoms in Co- and Ni-promoted MoS2-based hydrotreating catalysts. J Catal 2007;249:220–33.
[49] Katrib A, Benadda A, Sobczak JW, Maire G. XPS and catalytic properties of the bifunctional supported MoO_2(Hx)ac on TiO_2 for the hydroisomerization reactions of hexanes and 1-hexene. Appl Catal, A 2003;242:31–40.
[50] Baker MA, Gilmore R, Lenardi C, Gissler W. XPS investigation of preferential sputtering of S from MoS_2 and determination of MoSx stoichiometry from Mo and S peak positions. Appl Surf Sci 1999;150:255–62.
[51] Mérida-Robles J, Rodríguez-Castellón E, Jiménez-López A. Characterization of Ni, Mo and Ni–Mo catalysts supported on alumina-pillared α-zirconium phosphate and reactivity for the thiophene HDS reaction. J Mol Catal A: Chem 1999;145:169–81.
[52] Guichard B, Roy-Auberger M, Devers E, Legens C, Raybaud P. Aging of Co(Ni)MoP/Al_2O_3 catalysts in working state. Catal Today 2008;130:97–108.
[53] Kumar KS, Li W, Choi M, Kim SM, Kim J. Synthesis and lithium storage properties of MoS_2 nanoparticles prepared using supercritical ethanol. Chem Eng J 2016;285:517–27.
[54] Kubička D, Kaluža L. Deoxygenation of vegetable oils over sulfided Ni, Mo and NiMo catalysts. Appl Catal, A 2010;372:199–208.
[55] Kim SK, Han JY, Lee H-s, Yum T, Kim Y, Kim J. Production of renewable diesel via catalytic deoxygenation of natural triglycerides: comprehensive understanding of reaction intermediates and hydrocarbons. Appl Energy 2014;116:199–205.
[56] Snåre M, Kubičková I, Mäki-Arvela P, Eränen K, Murzin DY. Heterogeneous catalytic deoxygenation of stearic acid for production of biodiesel. Ind Eng Chem Res 2006;45:5708–15.
[57] Gao J, Wang Y, Ping Y, Hu D, Xu G, Gu F, et al. A thermodynamic analysis of methanation reactions of carbon oxides for the production of synthetic natural gas. RSC Adv 2012;2:2358–68.
[58] Zabarnick S, Widmor N. Studies of jet fuel freezing by differential scanning calorimetry. Energy Fuels 2001;15:1447–53.
[59] Chuck CJ, Donnelly J. The compatibility of potential bioderived fuels with Jet A-1 aviation kerosene. Appl Energy 2014;118:83–91.
[60] Bezergianni S, Dimitriadis A, Kalogianni A, Knudsen KG. Toward hydrotreating of waste cooking oil for biodiesel production. Effect of pressure, H_2/Oil ratio, and liquid hourly space velocity. Ind Eng Chem Res 2011;50:3874–9.
[61] Guzman A, Torres JE, Prada LP, Nuñez ML. Hydroprocessing of crude palm oil at pilot plant scale. Catal Today 2010;156:38–43.